Using MAT213 for Simulation of High-Speed Impacts of Composite Structures

Loukham Shyamsunder, Bilal Khaled, Canio Hoffarth and Subramaniam D. Rajan
School of Sustainable Engineering and the Built Environment, Arizona State University, Tempe, AZ
Robert K. Goldberg
NASA-GRC, Cleveland, OH
Kelly S. Carney and Paul DuBois
George Mason University, Fairfax, VA
Gunther Blankenhorn
LSTC, Livermore, CA

Abstract

A general purpose orthotropic elasto-plastic computational constitutive material model has been developed to predict the response of composites subjected to high velocity impact. The three-dimensional orthotropic elasto-plastic composite material model is being implemented in a special version of LS-DYNA® for solid elements as MAT213. In order to accurately represent the response of a composite, experimental stress-strain curves are utilized as input, allowing for a more general material model that can be used on a variety of composite applications. The experimental procedures are discussed in a companion paper. This paper documents the implementation, verification and validation of the material model using the T800-F3900 fiber/resin composite material, a commonly used composite in the aerospace industry.

Introduction

Composites have become popular mainly in the mechanical and the aerospace industries. In the design and analysis point of view of composites, simulations have started replacing expensive experiments. This can be attributed to the improvement in the computing power in the last few decades due to advances in both hardware and software. The modeling of composites required for the simulation has always been a challenge. Recently, a robust orthotropic elasto-plastic material model has been developed [Goldberg et al., 2015] with the joint effort of the FAA and NASA. The model is implemented as MAT213 [Hoffarth et al., 2016] in LS-DYNA [LSTC, 2017]. MAT213 has three components- deformation, damage and failure model. It is an orthotropic plasticity material model that is driven by tabulated experimental data. The deformation model requires tweleve stress-strain curves as input for a given temperature and strain-rate. Damage parameters required for the damage model are described in an upcoming publication [Khaled et al., 2018]. The failure model supports three failure criteria – Principal Strain Failure Criterion (PSFC), Tsai-Wu Failure Criterion (TWFC) and a Generalized Tabulated Failure Criterion (GTFC). In this paper, a brief background on the implementation of MAT213 is discussed, and later the verification and validation tests are presented.

Theoretical Background

The theory which is discussed in Goldberg et al. [2015] requires twelve distinct stress-strain curves as input to drive the deformation model. Considering 1, 2 and 3 as the principal material directions, the twelve stress-strain curves include (i) tension curves in the 1, 2, and 3 directions, (ii) compression curves in the 1, 2, and 3 directions, (iii) shear curves in the 1-2, 2-3, and 1-3 planes, and (iv) 45° off-axis tension or compression tests

curves in the 1-2, 2-3, and 1-3 principal material planes. If the composite exhibits rate and/or temperature dependencies, then these twelve curves may be generated at various temperature and strain rates.

The material model presented is a three-dimensional orthotropic elasto-plastic model which was developed [Hoffarth et al., 2016] to be general enough to support a large variety of composite architectures. The elasto-plastic deformation in the model is based on a general orthotropic constitutive relationship, represented by orthotropic elastic stiffness matrix as shown in Equation (1). The elastic moduli values to be used for Equation (1) are computed internally by MAT213 using initial yield stress and the specified initial yield strain.

$$\mathbf{C}=\mathbf{S}^{-1}=\begin{bmatrix} \frac{1}{E_{11}} & -\frac{\nu_{21}}{E_{22}} & -\frac{\nu_{31}}{E_{33}} & 0 & 0 & 0 \\ & \frac{1}{E_{22}} & -\frac{\nu_{32}}{E_{33}} & 0 & 0 & 0 \\ & & \frac{1}{E_{33}} & 0 & 0 & 0 \\ & & & \frac{1}{G_{23}} & 0 & 0 \\ & Sym & & & \frac{1}{G_{31}} & 0 \\ & & & & & \frac{1}{G_{12}} \end{bmatrix}^{-1} \tag{1}$$

The initiation and evolution of plasticity is dictated by the Tsai-Wu yield function which is shown in Equation (2) [Hoffarth et al., 2016; Goldberg et al., 2015]

$$f(\sigma)=-1+\begin{pmatrix} F_1 & F_2 & F_3 & 0 & 0 & 0 \end{pmatrix}\begin{bmatrix}\sigma_{11}\\ \sigma_{22}\\ \sigma_{33}\\ \sigma_{12}\\ \sigma_{23}\\ \sigma_{31}\end{bmatrix}+\begin{bmatrix}\sigma_{11}\\ \sigma_{22}\\ \sigma_{33}\\ \sigma_{12}\\ \sigma_{23}\\ \sigma_{31}\end{bmatrix}^{T}\begin{bmatrix} F_{11} & F_{12} & F_{13} & 0 & 0 & 0 \\ F_{12} & F_{22} & F_{23} & 0 & 0 & 0 \\ F_{13} & F_{23} & F_{33} & 0 & 0 & 0 \\ 0 & 0 & 0 & F_{44} & 0 & 0 \\ 0 & 0 & 0 & 0 & F_{55} & 0 \\ 0 & 0 & 0 & 0 & 0 & F_{66} \end{bmatrix}\begin{bmatrix}\sigma_{11}\\ \sigma_{22}\\ \sigma_{33}\\ \sigma_{12}\\ \sigma_{23}\\ \sigma_{31}\end{bmatrix} \tag{2}$$

where F_{ij} are the yield function coefficients which represent the yield stress contribution in the different coordinate directions. The yield function coefficients are initially computed based on the initial yield stress values to determine the onset of plasticity as shown in Equation (3), (4), (5) and (6). In order to check for the evolution of plasticity, the coefficients are computed corresponding to the current yield stress (flow stress).

$$\begin{aligned} F_1&=\frac{1}{\sigma_{11}^T}-\frac{1}{\sigma_{11}^C} & F_{11}&=\frac{1}{\sigma_{11}^T\sigma_{11}^C} & F_{44}&=\frac{1}{\sigma_{12}^2}\\ F_2&=\frac{1}{\sigma_{22}^T}-\frac{1}{\sigma_{22}^C} & F_{22}&=\frac{1}{\sigma_{22}^T\sigma_{22}^C} & F_{55}&=\frac{1}{\sigma_{23}^2}\\ F_3&=\frac{1}{\sigma_{33}^T}-\frac{1}{\sigma_{33}^C} & F_{33}&=\frac{1}{\sigma_{33}^T\sigma_{33}^C} & F_{66}&=\frac{1}{\sigma_{31}^2} \end{aligned} \tag{3}$$

$$F_{12} = \frac{2}{\left(\sigma_{12}^{45}\right)^2} - \frac{F_1 + F_2}{\sigma_{12}^{45}} - \frac{1}{2}\left(F_{11} + F_{22} + F_{44}\right) \tag{4}$$

$$F_{23} = \frac{2}{\left(\sigma_{23}^{45}\right)^2} - \frac{F_2 + F_3}{\sigma_{23}^{45}} - \frac{1}{2}\left(F_{22} + F_{33} + F_{55}\right) \tag{5}$$

$$F_{13} = \frac{2}{\left(\sigma_{31}^{45}\right)^2} - \frac{F_1 + F_3}{\sigma_{31}^{45}} - \frac{1}{2}\left(F_{11} + F_{33} + F_{66}\right) \tag{6}$$

The current yield stresses are characterized by the stress-strain curves in the corresponding material directions which is input into the material model. The initial yield stresses are defined based on the user specified initial yield strain values which is also an input into MAT213. MAT213 is based on a non-associative flow law requiring a separate flow surface, defined by a general quadratic plastic potential function. The plastic potential function and description of the process for determining the flow rule coefficients is presented in Goldberg et al. [2015], with the plastic potential shown in Equation (7).

$$h = \sqrt{H_{11}\sigma_{11}^2 + H_{22}\sigma_{22}^2 + H_{33}\sigma_{33}^2 + 2H_{12}\sigma_{11}\sigma_{22} + 2H_{23}\sigma_{22}\sigma_{33} + 2H_{31}\sigma_{33}\sigma_{11} + H_{44}\sigma_{12}^2 + H_{55}\sigma_{23}^2 + H_{66}\sigma_{31}^2} \tag{7}$$

where the H_{ij} are the flow rule coefficients and σ_{ij} are the current stresses in the material (not yield stresses). In short, the flow law is defined in terms of the plastic strain rate $\left(\dot{\varepsilon}^p\right)$, plastic multiplier $\left(\lambda\right)$, plastic potential function $\left(h\right)$ and stresses $\left(\boldsymbol{\sigma}\right)$ as shown in Equation (8).

$$\dot{\boldsymbol{\varepsilon}}^p = \dot{\lambda}\frac{\partial h}{\partial \boldsymbol{\sigma}} \tag{8}$$

where the plastic strains are related to the plastic Poisson's ratios ν_{ij}^p as $\nu_{ij}^p = -\frac{\dot{\varepsilon}_{jj}^p}{\dot{\varepsilon}_{ii}^p}$, which are used to compute the flow rule coefficients [Hoffarth et al., 2017]. Although, the deformation model takes care of the non-linear stress-strain behavior of the material, the elastic unloading is handled by the damage model. The damage model is taken care of by the damage tensor $\mathbf{M}$, as shown in Equation (9). $\boldsymbol{\sigma}$ represents the true stress which is obtained from the experiments, and $\boldsymbol{\sigma}_{\mathbf{eff}}$ represents the effective stress which corresponds to the undamaged material.

$$\boldsymbol{\sigma} = \mathbf{M}\boldsymbol{\sigma}_{\mathbf{eff}} \tag{9}$$

$\mathbf{M}$ is a diagonal matrix which is given by Equation (10). The terms in $\mathbf{M}$ are dependent on the plastic strains in the material, and are determined experimentally [Khaled et al., 2018].

$$\mathbf{M} = \begin{bmatrix} \mathbf{M}_{11} & 0 & 0 & 0 & 0 & 0 \\ 0 & \mathbf{M}_{22} & 0 & 0 & 0 & 0 \\ 0 & 0 & \mathbf{M}_{33} & 0 & 0 & 0 \\ 0 & 0 & 0 & \mathbf{M}_{44} & 0 & 0 \\ 0 & 0 & 0 & 0 & \mathbf{M}_{55} & 0 \\ 0 & 0 & 0 & 0 & 0 & \mathbf{M}_{66} \end{bmatrix} \tag{10}$$

Three potential criteria may be used to determine the onset of failure in the material. The PSFC checks whether the strain in the principal directional exceeds the ultimate failure strain obtained from the experiments [Khaled et al., 2017] in the respective direction. All the experimental data [Khaled et al., 2017] are obtained using coupon testing on a hydraulic test frame. Load cells built into the test frames are used to obtain force data. Digital image correlation (DIC) is used to capture the strain field throughout the duration of the experiment. The TWFC checks whether Equation (2) is satisfied where the coefficients, F_{ij}, are computed using Equation (3), (4), (5) and (6) using the failure strength in the respective component. The GTFC [Goldberg et al., 2017] requires the failure surface in in-plane and out-of-plane in the form of tabular data as input.

Verification test

The verification of the material model was first done using single element models with the deformation, damage and failure models active. Multi-element models were then made with the same geometry as those used in the experiments [Khaled et al., 2017, 2018]. A subset of the verification tests run using the deformation and failure models are presented here. The material properties of T800/F3900 obtained from the experiments at quasi-static rate and room temperature are shown in Table 1.

Table 1. Material Properties

Property	Value (Tensile)	Value (Compressive)
1-direction modulus (E_{11}, psi)	23.5×10^6	18.7×10^6
2-direction modulus (E_{22}, psi)	1.07×10^6	1.12×10^6
3-direction modulus (E_{33}, psi)	9.66×10^5	1.04×10^6
1-2 plane shear modulus (G_{12}, psi)	5.80×10^5	
2-3 plane shear modulus (G_{23}, psi)	3.26×10^5	
1-3 plane shear modulus (G_{13}, psi)	3.48×10^5	
Poisson's ratio (ν_{12})	0.317	0.342
Poisson's ratio (ν_{23})	0.484	0.728
Poisson's ratio (ν_{13})	0.655	0.578
Poisson's ratio (ν_{21})	0.0168	0.0207
Poisson's ratio (ν_{32})	0.439	0.676
Poisson's ratio (ν_{31})	0.027	0.032
Density (ρ, slugs/in^3)	1.457×10^{-4}	

Tension 1-Direction Verification Test

The schematic diagram of the model used for the simulation is shown in Figure 1. The model dimensions in inches are also shown. In Figure 1a, "t" represents the thickness of the coupon. The green colored line represents the direction of the fiber. Figure 1b shows the finite element (FE) model. The FE model is comprised of 64 elements in total, with one element through the thickness. In order to simulate the tensile test, the nodes at

the left edge were restrained from translation in the x-direction except for the middle two nodes through the thickness which were restrained from translation in the x, y and z-directions. Velocity was applied to the nodes on the right edge which is represented by the arrows pointing in the positive x-direction.

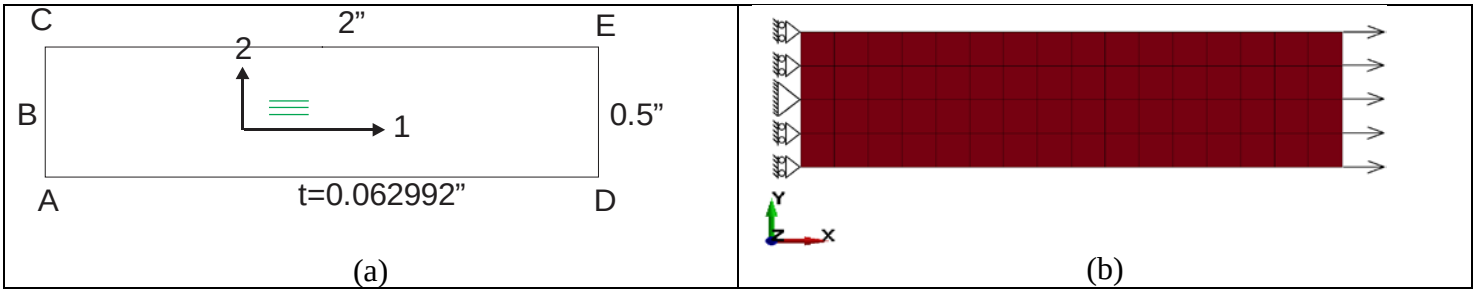

Figure 1. Tension 1-direction (a) model schematic diagram (b) FE model

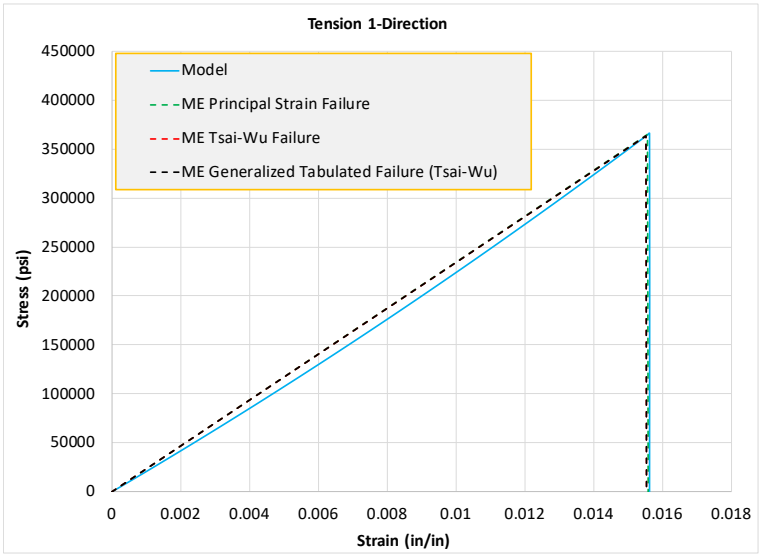

Figure 2. Tension 1-direction stress-strain plot

Three different simulations were run using each of the failure criteria. The middle four elements were considered for the post-processing. The average of the stress-strain data of these four elements were taken into consideration. The stress-strain curves are shown in Figure 2. The “Model” plot refers to the curve obtained from experiments which is fed into MAT213. “ME Principal Strain Failure” plot represents the simulation run with PSFC activated. “ME Tsai-Wu Failure” plot represents the simulation run with TWFC activated. “ME Generalized Tabulated Failure” represents the simulation run using GTFC. Since, there were not enough failure surface points available, fictitious data derived using Tsai-Wu failure criterion was used to complete the tabulated failure surface. The drop in each curve to zero stress value implies that failure has occurred. It can be observed that MAT213 predicted the response fairly well.

Compression 3-Direction Verification Test

The model used for the test was a cube. The schematic diagram of the model used for this simulation is shown in Figure 3. The model dimensions in inches are also shown in Figure 3a. There are 64 elements in the FE model. There are four elements through the thickness, and hence five nodes. All the nodes on the left face are restrained from translation in the x-direction as shown in Figure 3b except for the node at the center which is restrained from translation in the x, y and z-directions. The nodes on the right face is subjected to velocity towards the negative x-direction.

Figure 3. Compression 3-direction (a) model schematic diagram (b) FE model

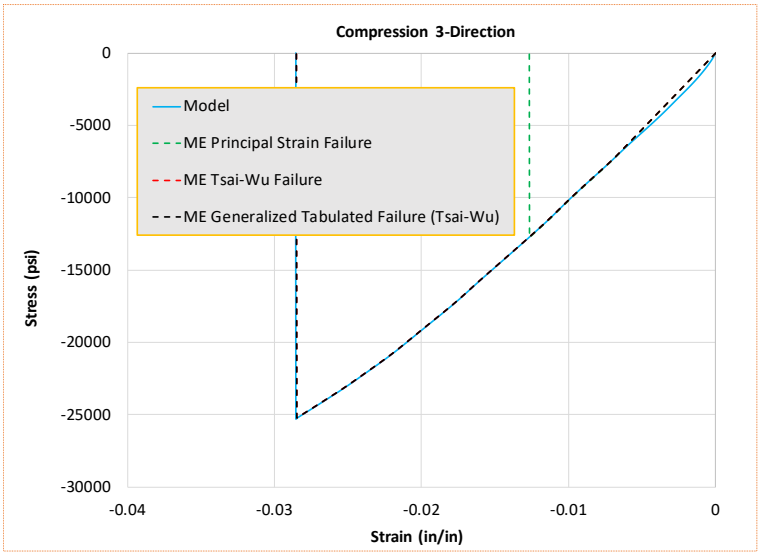

Figure 4. Compression 3-direction stress-strain plot

Similar to the previous verification test, three different simulations were run using each of the failure criteria. The middle 8 elements were considered for the post processing. The average of the stress-strain data of the middle 8 elements were taken into consideration. The stress-strain curves are shown in Figure 4. Response obtained using TWFC and GTFC fairly matched the input curve. The response obtained using PSFC failed prematurely due strain evolving in the 2-direction because of high Poisson's ratio (ν_{23}).

Validation Test

The validation test for the material model was carried out using a ballistic plate impact test. Previous validation test results have been presented in Hoffarth et al. [2017] which involves a unidirectional composite plate subjected to low velocity impact. This section presents the impact test carried out on composite plate subjected to a higher velocity impact. The impact test was carried out at NASA-Glenn Research Center (NASA-GRC). The plate is made of the T800/F3900 composite with a 16 ply lay up $[(0/90/45/-45)_2]_S$. The panel has dimensions of 12" x 12" x 0.122" and a mass of 434.4 g. Figure 5a shows the front of the plate clamped using bolts. Figure 5c shows the projectile before the test is done on it. The projectile is made of Al-2024 with a mass of 50 g. The projectile was fired using a pressure gun.

The impact velocity of the projectile was recorded as 155 ft/s. The impact was perpendicular and center to the plate. DIC was used to track the out-of-plane (z-direction) displacement and in-plane strains on the entire back

surface of the plate. Figure 5b shows the front of the plate after the impact. Figure 5d shows the speckled projectile after the test. The speckling was done on the projectile to track its speed and orientation. The projectile did not penetrate the plate. Figure 6 shows the ultrasonic scan images of the plate before and after the impact. These images were provided by NASA-GRC. The small grey portion at the center of Figure 6b implies that there is insignificant damage in the plate due to the impact. If the damage was significant, the grey portion would have been darker and larger in size.

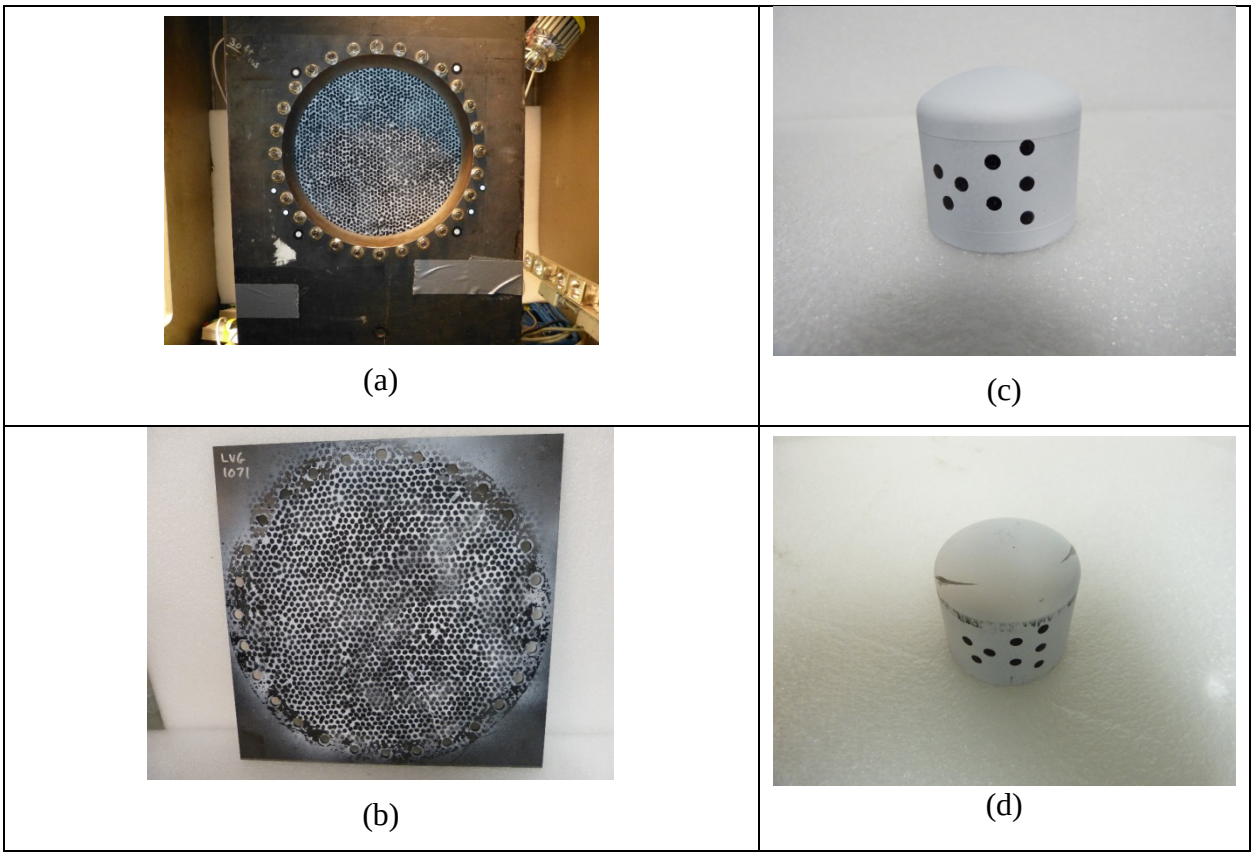

Figure 5. Impact structural test (a) front of the plate on with a 10” circular clamping pattern support before the impact (b) plate after the impact (c) Al-2024 projectile before the test (d) Al-2024 projectile after the test

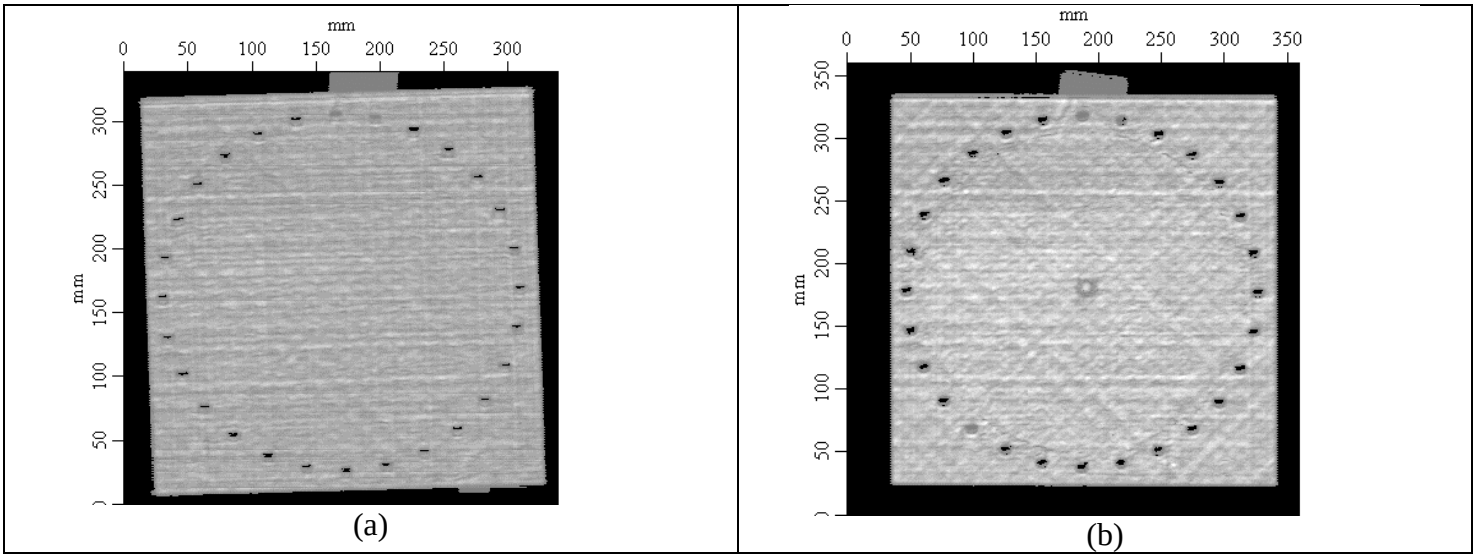

Figure 6. Ultrasonic scan images of the plate (a) before the impact (b) after the impact

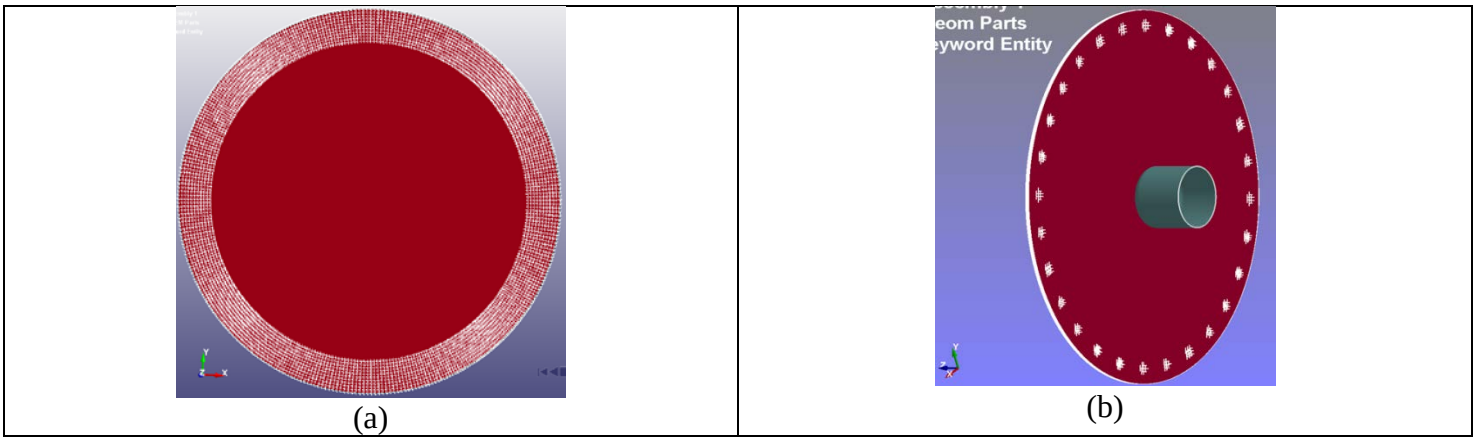

Figure. 7. LS-DYNA finite element model (a) back view, (b) side view

To simulate the impact test, a FE model was created (Figure 7). The nodes at the clamp around the plate were restrained from translation in the out-of-plane mode (highlighted in Figure 7a). The nodes at the hole were fixed from translation in the in-plane mode (highlighted in Figure 7b). The plate in the finite element model has 370,184 8-noded hexahedral elements for the plies with 16 elements through the thickness to represent each ply (16 plies). These 16 plies were modeled using MAT213 with the respective orientation of the fibers. Cohesive zone elements, with zero thickness, were used between composite plies to capture any delamination that may have occurred. The cohesive elements were modeled using 8-noded hexahedral elements with MAT138. The properties used for the cohesive elements were taken from Pratap [2010]. The properties used for the cohesive elements are tabulated in Table 2. The projectile is modeled using 17,040 8-noded hexahedral elements. The projectile is modeled as aluminum using MAT024. Table 3 enlists the material properties used for MAT_024. CONTACT_ERODING_SINGLE_SURFACE and CONTACT_ERODING_SURFACE_TO_SURFACE contact definitions were used.

Table 2. MAT138 properties

Model Parameter	**Value**
Mass density (slugs/in^3)	8.5(10^{-8})
EN (lb/in)	6.16(10^8)
ET (lb/in)	6.16(10^8)
GIC (lb/in)	4.28
GIIC (lb/in)	14.50
T (psi)	4000
S (psi)	8000

Table 3. MAT024 Properties

Model Parameter	**Value**
Mass density (slugs/in^3)	2.539(10^{-4})
E (psi)	10.30(10^6)
ν	0.334
Yield Stress, SIGY (psi)	42500
Tangent Modulus, ETAN (psi)	42000

Since no penetration of the projectile through the plate was observed during the experiment, and also since there was no significant damage induced in the plate, MAT213 was run with the damage model and the failure model inactive. In order to compare the result obtained from the finite element simulation and the experiment, the out-of-plane displacement of the central node at the back of the plate was used as the metric. The out-of-plane displacements plotted against time is shown in Figure 8. "Experiment-Center" is the out-of-plane displacement at the central node on the back side of the plate obtained from the experiment. "MAT213-Center" corresponds to the displacement obtained from the simulation. It can be observed that the simulation result fairly matches the experimentally obtained result.

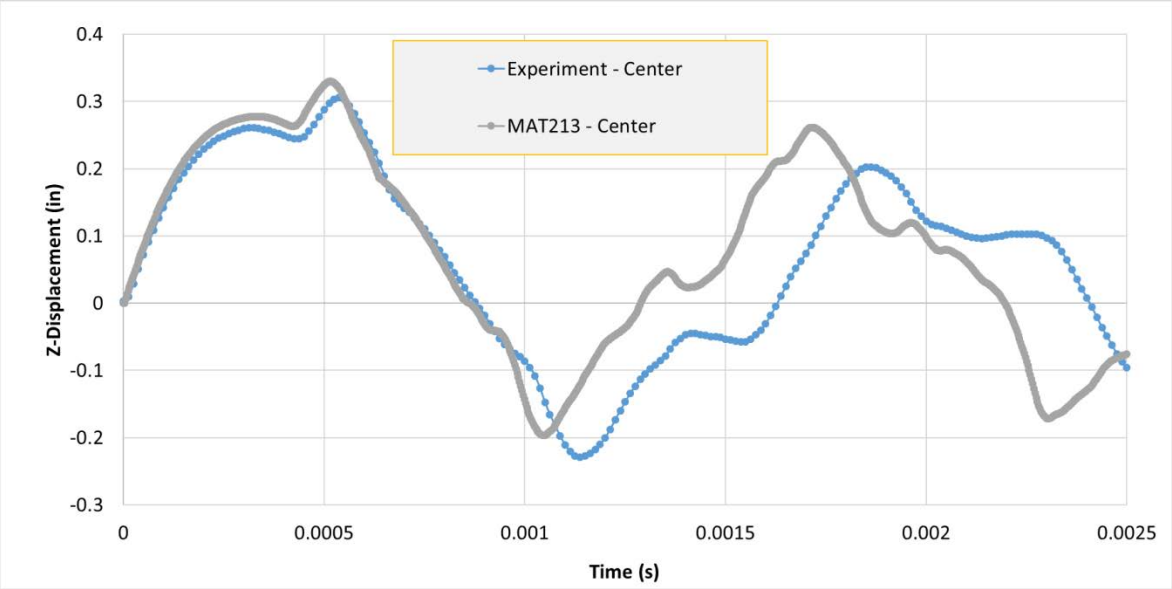

Figure 8. Comparison of out-of-plane (z) displacement versus time plot obtained from MAT213 simulations and the experiment

Additionally, the contour of the out-of-plane displacement was also compared. Figure 9 shows the contour of the maximum out-of-plane displacement. Figure 9a shows the contour obtained from the DIC during the experiment. Figure 9b shows the finite element model contour at the same time of 0.0005s with the same scale. Here also, it can be observed that the displacement field of the simulation model is similar to that of the experiment.

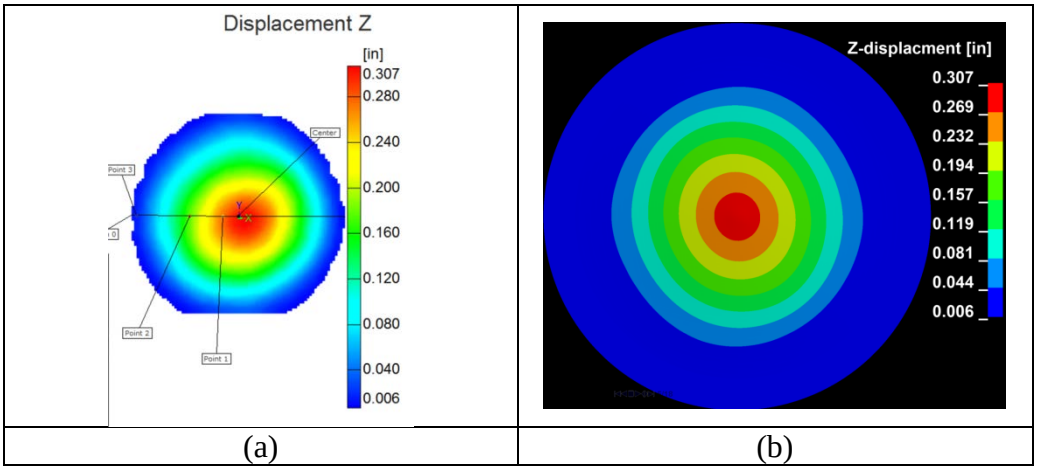

Figure 9. Contour of the maximum out of plane displacement obtained during (a) experiment, and (b) MAT213 simulation

Conclusions

The implementation, verification and the validation of a general orthotropic elasto-plastic three-dimensional material model with tabulated data input which has been implemented into LS-DYNA is presented. The impact test of a plate made of composite material is also presented as part of the validation test. It is shown that the material model can accurately predict the response of the plate subjected to an impact. Future work involves carrying out more validation test with higher velocities of impact which would induce significant damage and also the projectile penetrating the plate.

Acknowledgements

Authors Shyamsunder, Khaled, Hoffarth and Rajan gratefully acknowledge the support of (a) the Federal Aviation Administration through Grant #12-G-001 titled "Composite Material Model for Impact Analysis", William Emmerling, Technical Monitor, and (b) NASA through Contract Number: NN15CA32C titled "Development and Implementation of an Orthotropic Plasticity Progressive Damage Model for Transient Dynamic/Impact Finite Element Analysis of Composite Structures", Robert Goldberg, Contracting Officer Representative.

References

Goldberg, R., Carney, K., DuBois, P., Hoffarth, C., Harrington, J., Rajan, S.D. and Blankenhorn, G. (2015). "Development of an Orthotropic Elasto-Plastic Generalized Composite Material Model Suitable for Impact Problems", ASCE J of Aerospace Engineering, DOI: 10.1061/(ASCE)AS.1943-5525.0000580.

Goldberg, R., Carney, K., DuBois, P., Hoffarth, C., Khaled, B., Shyamsunder, L., Rajan, S.D. and Blankenhorn, G. (2017). "Implementation of a Tabulated Failure Model Into a Generalized Composite Material Model Suitable for Use in Impact problems", American Society for Composites, Thirty-Second Technical Conference, 2017, Purdue University, West Lafayette, Indiana, USA.

Hoffarth, C., Rajan, S.D., Goldberg, R., Carney, K., DuBois, P. and Blankenhorn, G. (2016). Implementation and Validation of a Three-Dimensional Material Model for Orthotropic Composites, *Composites Part A: Applied Science and Manufacturing, 91*(1), 336-350.

Hoffarth, C., Khaled, B., Shyamsunder, L., Rajan, S.D., Goldberg, R., Carney, K., DuBois, P. and Blankenhorn, G. (2017). "Verification and Validation of a Three-Dimensional Orthotropic Plasticity Constitutive Model Using a Unidirectional Composite", Fibers 5(1), 1-13.

Khaled, B., Shyamsunder, L., Hoffarth, C., Rajan, S.D, Goldberg, R., Carney, K., DuBois, P., and Blankenhorn, G. (2017). "Experimental Characterization of Composites to Support an Orthotropic Plasticity Material Model", J of Composite Materials, DOI: 10.1177/0021998317733319, August 2017.

Khaled, B., Shyamsunder, L., Hoffarth, C., Rajan, S.D, Goldberg, R., Carney, K., DuBois, P., and Blankenhorn, G. (2018). "Damage Characterization of Composites to Support an Orthotropic Plasticity Model", manuscript in preparation.

LSTC (2017). LS-DYNA R8, http://lstc.com/products/ls-dyna

Pratap, N.N. (2010). "Rate sensitivity of the interlaminar fracture toughness of laminated composites". Wichita State university. http://soar.wichita.edu/handle/10057/3699.